Discrete dislocation plasticity and crack tip fields in single crystals

van der Giessen, E.; Deshpande, V.S.; Cleveringa, H.H.M.; Needleman, A.

Published in:
Journal of the Mechanics and Physics of Solids

DOI:
10.1016/S0022-5096(01)00040-0

Publication date:
2001


PERGAMON

Journal of the Mechanics and Physics of Solids
49 (2001) 2133–2153

JOURNAL OF THE
MECHANICS AND
PHYSICS OF SOLIDS

www.elsevier.com/locate/jmps

Discrete dislocation plasticity and crack tip fields in single crystals

E. Van der Giessen[a,*], V.S. Deshpande[b], H.H.M. Cleveringa[a], A. Needleman[b]

[a] *Micromechanics of Materials Group, Koiter Institute Delft, Delft University of Technology, Mekelweg 2, 2628 CD Delft, The Netherlands*
[b] *Brown University, Division of Engineering, Providence, RI 02912, USA*

Abstract

Small-scale yielding around a stationary plane strain mode I crack is analyzed using discrete dislocation plasticity. The dislocations are all of edge character, and are modeled as line singularities in a linear elastic material. Superposition is used to represent the solution in terms of analytical fields for edge dislocations in a half-space and a numerical image solution that enforces the boundary conditions. The description of the dislocation dynamics includes the lattice resistance to dislocation motion, dislocation nucleation, interaction with obstacles and annihilation. A model planar crystal with three slip systems is considered. Two slip system orientations are analyzed that differ by a 90° rotation. The non-hardening, single crystal plasticity continuum slip solution of Rice (Mech. Mater. 6 (1987) 317) for this model crystal predicts that slip and kink bands emerge for both crystal geometries, while Drugan (J. Mech. Phys. Solids 49 (2001) 2155) has obtained kink band free solutions. For a reference set of parameter values, kink band free solutions are found in one orientation while the emergence of kink bands is seen in the other orientation. However, lowering the dislocation source density suppresses the formation of kink bands in this orientation as well. In all calculations, the opening stress in the immediate vicinity of the crack tip is much larger than predicted by continuum slip theory.

Keywords: A. Crack tip plasticity; A. Dislocations; A. Fracture mechanisms; B. Crystal plasticity

* Corresponding author. Present address: University of Groningen, Department of Applied Physics, 9747 AG Groningen, The Netherlands. Tel.: +31-15-278-6500; fax: +31-15-278-2150.
E-mail address: Giessen@phys.rug.nl (E. Van der Giessen).

0022-5096/01/$ - see front matter
PII: S0022-5096(01)00040-0

1. Introduction

In ductile metals, the work required to break atomic bonds is only a small fraction of the macroscopic work to fracture since the major contribution comes from plastic dissipation. Hence, plastic flow in the vicinity of a crack tip is the key for determining the crack growth resistance of ductile metals. Indeed, the analysis of asymptotic crack tip fields in isotropic strain hardening solids by Hutchinson (1968) and Rice and Rosengren (1968) provided the impetus for the development of non-linear fracture mechanics.

These HRR fields are often appropriate to model the crack-tip fields at a macroscopic scale, averaging out over many grains. When the crack opening is much less than the grain size and when zooming into the near-tip region, the crack-tip fields are contained in a single crystal. At this scale, the discreteness of slip systems plays a major role in setting the plastic deformation field. Within the framework of continuum slip theory, Rice (1987) analyzed near-tip tensile crack fields for non-hardening plastic crystals, neglecting the geometry changes. Subsequently, Saeedvafa and Rice (1989) extended the small deformation analysis to power-law hardening crystals while Cuitiño and Ortiz (1992) carried out a numerical solution fully accounting for finite deformations. The single crystal near-tip fields are quite different from the HRR fields in an isotropic plastic solid and depend on the orientation of the slip systems relative to the crack plane.

Rice's (1987) solution for the near-tip stress fields of non-hardening plastic crystals consists of sectors of constant stress, with concentrated deformation on the sector boundaries either in a slip band (with the slip direction along the band) or in a kink band (where the slip direction is perpendicular to the band). These features are reflected in the strain hardening (Saeedvafa and Rice, 1989) and finite deformation solutions (Cuitiño and Ortiz, 1992), but not simply. However, the non-hardening plasticity solutions are not unique. One feature of the non-hardening solutions of Rice (1987) is that they necessarily involve localized kink bands. Drugan (2001) has recently obtained solutions that involve localized slip only.

Cleveringa et al. (2000) recently carried out an analysis in which one zooms in even further and the discreteness of the dislocations is accounted for. That is, plasticity was described in terms of the collective motion of large numbers of discrete dislocations. The dislocations were found to play a dual role. On the one hand, the dissipation associated with dislocation motion gave rise to a toughness much higher than that associated with the work of creating a new surface. On the other hand, it was the local stress concentration associated with discrete dislocation patterning that led to stress levels much higher than the yield stress and indeed high enough to cause atomic separation. It was found that, away from the very near crack tip region, the stress variation appeared consistent with the main features of Rice's (1987) continuum slip solution, although a detailed comparison was not attempted.

Here, we focus attention on stationary cracks and carry out such a detailed comparison between the discrete dislocation predictions and those of the continuum slip theory. As in Cleveringa et al. (2000), a boundary value problem for small-scale yielding of a mode I crack in plane strain is formulated and solved. The stresses and strains are written as superpositions of fields due to the discrete dislocations, which are singular inside the body, and image fields that enforce the boundary conditions. The long-range

interactions between dislocations are accounted for through the continuum elasticity fields, while drag during dislocation motion, interactions with obstacles, and dislocation nucleation and annihilation are accounted for through a set of constitutive rules. A density of two-dimensional Frank–Read sources and of obstacles to dislocation motion are randomly distributed in the neighborhood of the crack tip. There is no special dislocation nucleation from the crack tip. The solutions obtained here are compared with the non-hardening continuum slip solutions of Rice (1987) and Drugan (2001).

2. Problem formulation and method of analysis

The formulation and numerical methods follow those in Cleveringa et al. (2000), where further details and additional references are given. We consider an infinitely long crack in a two-dimensional single crystal subjected to far-field mode I loading. The orientation of the crack is taken to be symmetric to the slip planes in the crystal, so that we need to consider only half of the crystal. Plasticity is assumed to be confined to a rectangular window of 10 μm × 12.5 μm inside which dislocations are treated discretely, see Fig. 1a. In this two-dimensional analysis, we consider three slip systems, so that there is a redundancy in available slip systems, as for three-dimensional fcc and bcc crystals. Two crystallographic orientations are studied (Fig. 1b). One orientation is such that the slip planes make angles $\phi^{(\alpha)} = (-60°, 0, +60°)$ with the crack plane $x_2 = 0$; we shall refer to this case as the fcc-like orientation. The other will be referred to as the bcc-like orientation for which the crystal is rotated 90°: $\phi^{(\alpha)} = (+30°, 90°, -30°)$.

Loading is prescribed in terms of displacements corresponding to the isotropic elastic mode I singular field remote from the crack tip. With Cartesian coordinates measured from the tip of the crack, the displacement components on the remote boundary are prescribed to be

$$u_1 = \frac{K_\mathrm{I}}{\mu}\sqrt{\frac{r}{2\pi}}\cos\frac{\theta}{2}\left(1 - 2\nu + \sin^2\frac{\theta}{2}\right), \tag{1}$$

$$u_2 = \frac{K_\mathrm{I}}{\mu}\sqrt{\frac{r}{2\pi}}\sin\frac{\theta}{2}\left(2 - 2\nu - \cos^2\frac{\theta}{2}\right), \tag{2}$$

where

$$r = \sqrt{x_1^2 + x_2^2}, \qquad \theta = \tan^{-1}\left(\frac{x_2}{x_1}\right), \tag{3}$$

$\mu = E/2(1+\nu)$ and K_I is the mode I stress intensity factor.

Although attention is confined to stationary cracks, there is a single cohesive surface (Needleman, 1990) that extends over a distance of x_c in front of the initial crack. Along the cohesive surface (Rose et al., 1981),

$$T_\mathrm{n}(\Delta_\mathrm{n}) = -\sigma_\mathrm{max}\frac{\Delta_\mathrm{n}}{\delta_\mathrm{n}}\exp\left(-\frac{\Delta_\mathrm{n}}{\delta_\mathrm{n}} + 1\right) \quad \text{for } 0 < x_1 < x_\mathrm{c} \tag{4}$$

with T_n the normal traction along the cohesive surface and $\Delta_\mathrm{n} = 2u_2(x_1, 0)$, the normal opening. Since the focus is on the crack-tip fields prior to crack growth, the calculations

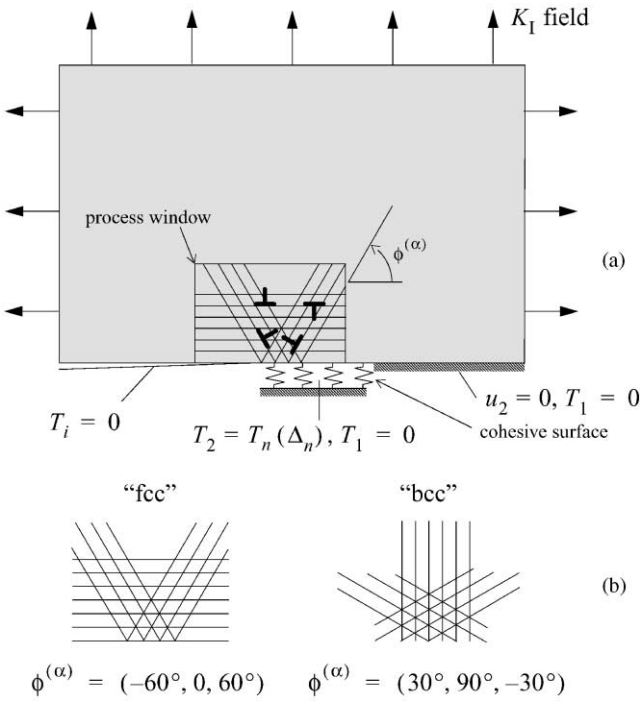

Fig. 1. (a) Small-scale yielding analysis under mode I conditions with discrete dislocations moving inside a process window. Because of symmetry, only half the problem needs to be analyzed. The cohesive surface ahead of the initial crack is used to describe crack growth. (b) The two orientations that are considered in the analysis.

are carried out using $\sigma_{\max} = 3$ GPa and $\delta_n = 10b$. Ahead of the cohesive surface, symmetry conditions are prescribed.

The elastic response of the material is taken to be isotropic, with shear modulus $\mu = 26.3$ GPa and Poisson's ratio $\nu = 0.3$. Plastic deformation is assumed to occur by the motion of edge dislocations only, with Burgers vector $b = 0.25$ nm. Initially, the crystal is assumed to be free of mobile dislocations, but to contain a random distribution of dislocation sources and point obstacles. The sources mimic Frank–Read sources and generate a dislocation dipole when the Peach–Koehler force exceeds a critical value of $\tau_{\text{nuc}}b$ during a period of time t_{nuc}. The obstacles, which could be small precipitates or forest dislocations, pin dislocations and will release them once the Peach–Koehler force attains the obstacle strength $\tau_{\text{obs}}b$. Annihilation of two dislocations with opposite Burgers vector occurs when they approach each other within a critical annihilation distance L_e. Only dislocation glide is incorporated, and it is assumed to be governed by a linear drag relation between the dislocation velocity and the Peach–Koehler force.

In most of the calculations here, we use a reference set of dislocation parameters having $\tau_{\text{nuc}} = 50$ MPa, $\tau_{\text{obs}} = 150$ MPa, $t_{\text{nuc}} = 10$ ns and an annihilation distance $L_e = 6b$ with a source density of 78 μm^{-2} and an obstacle density of 200 μm^{-2} for both crystal

orientations. All slip planes are equally spaced in the process window with a spacing of $86b$. To explore the sensitivity of the deformation fields to the availability of dislocation sources, results are also presented for the bcc-like orientation with the dislocation source density lowered to 46 μm^{-2} and with all other parameters unchanged.

The stress and deformation fields are obtained in an incremental manner as described in detail in (Cleveringa et al., 2000). In each time increment, (i) the dislocation distribution is updated according to the above rules for motion, generation, annihilation and pinning, and (ii) the increment in the fields is solved from the incremental version of the virtual work equation

$$\int_V \sigma_{ij}\delta\varepsilon_{ij}\,\mathrm{d}V - \frac{1}{2}\int_{S_{\mathrm{coh}}} T_i\delta\Delta_i\,\mathrm{d}S = \int_{S_{\mathrm{ext}}} T_i\delta u_i\,\mathrm{d}S \tag{5}$$

for this problem. Here, V is the volume of the region analyzed, S_{ext} is the external surface and S_{coh} is the surface across which cohesive tractions operate. Further, σ_{ij} are the components of the stress tensor, and

$$\varepsilon_{ij} = \tfrac{1}{2}(u_{i,j} + u_{j,i}), \qquad T_i = \sigma_{ij}v_j, \tag{6}$$

with v_i the components of the unit outward normal on S_{coh} or S_{ext}. The factor $\frac{1}{2}$ in (5) stems from the fact that, by virtue of symmetry, only half of the work in the cohesive surface contributes to the work in the region analyzed. For the purpose of solving these equations, the velocity, strain-rate and stress-rate fields are written as the superposition of two fields,

$$\dot{u}_i = \tilde{\dot{u}}_i + \hat{\dot{u}}_i, \qquad \dot{\varepsilon}_{ij} = \tilde{\dot{\varepsilon}}_{ij} + \hat{\dot{\varepsilon}}_{ij}, \qquad \dot{\sigma}_{ij} = \tilde{\dot{\sigma}}_{ij} + \hat{\dot{\sigma}}_{ij} \tag{7}$$

as in Van der Giessen and Needleman (1995). The ($\tilde{}$) fields are the sum of the fields of the individual dislocations, in their current configuration, and give rise to tractions $\tilde{T}_i$ and displacements $\tilde{U}_i$ on the boundary of the body. The individual dislocation fields are those for an edge dislocation in a traction-free half-space (Freund, 1994), with the traction-free surface corresponding to the crack plane $x_2 = 0$. The ($\hat{}$) fields represent the image fields that correct for the actual boundary conditions.

The change in potential energy of the body due to infinitesimal variations of the position of the kth dislocation is given by the Peach–Koehler force,

$$f^{(k)} = n_i^{(k)}\left(\hat{\sigma}_{ij} + \sum_{m\neq k}\sigma_{ij}^{(m)} + \Sigma_{ij}^{(k)}\right) b_j^{(k)}. \tag{8}$$

Here, $n_i^{(k)}$ is the slip plane normal, $b_j^{(k)}$ is the Burgers vector and $\Sigma_{ij}^{(k)}$ is the image field on dislocation k due to the traction-free surface, i.e., the difference between the half-space and infinite medium fields.[1] The direction of the Peach–Koehler force is in the slip plane and normal to the dislocation line.

[1] This term was omitted in Cleveringa et al. (2000). In calculations carried out here, this term had only a small effect on the dislocation structures that develop for the fcc-like orientation, while results for the bcc-like orientation were found to be quite sensitive to the inclusion of this term.

3. Results

3.1. Rice's (1987) continuum slip analysis

Rice (1987) constructed non-hardening, single-crystal continuum plasticity solutions for crack tip fields in fcc and bcc crystals with the crack plane being (0 1 0). The solutions in Rice (1987) are readily modified for the slip system orientations of the model crystal geometries considered here (Fig. 1b).

Taking the critical resolved shear stress on all three slip systems to have the same value τ_0, we find the yield surfaces for the two orientations as shown in Fig. 2. Here, the values of τ_0 are taken to be the same for the two orientations, so that the yield surfaces are identical since the orientations differ by exactly 90°. As in Rice (1987), there is a solution such that the stress state near the tip is uniform in each of four angular sectors A–D and jumps discontinuously across sector boundaries, as illustrated in Fig. 2b. The full stress states are listed in Table 1. Inside each sector, the stress state is on the yield surface, so that all sectors yield. More precisely, the stress states are at yield surface vertices, with two slip systems active in each sector.

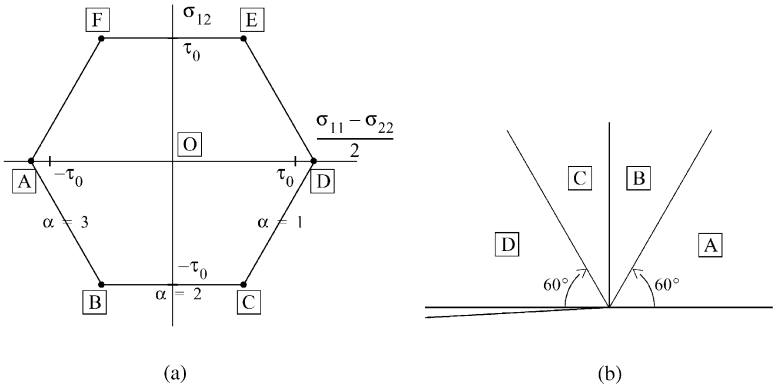

Fig. 2. (a) Yield surface according to continuum plasticity for the two crystal orientations considered here (see Fig. 1b). (b) The four angular sectors around the crack tip inside which the stress state is uniform (see Table 1). The letters indicate the stress states on the yield surface in (a).

Table 1
Stress states in the four sectors of Fig. 2 according to Rice's (1987) solution for the two orientations shown in Fig. 1b

Sector	σ_{22}/τ_0	σ_{11}/τ_0	σ_{12}/τ_0
A	$10/\sqrt{3}$	$2\sqrt{3}$	0
B	$7/\sqrt{3}$	$5/\sqrt{3}$	-1
C	$\sqrt{3}$	$5/\sqrt{3}$	-1
D	0	$4/\sqrt{3}$	0

For true fcc and bcc crystals (Rice, 1987), the sectors are the same, while the stresses are slightly different, but it bears emphasis that for the present fcc- and bcc-like orientations the two solutions are identical. The interpretations of the two solutions are, however, quite different. In the fcc-like orientation, $\phi^{(\alpha)} = (-60°, 0, +60°)$, the A–B and C–D sector boundaries are parallel to slip planes, while the B–C boundary is normal to the $\phi^{(2)} = 0$ planes. Normality of plastic flow dictates that plastic flow will tend to localize in shear along the A–B and C–D sector boundaries and will occur as a kink band at 90°, parallel to the B–C boundary. For the bcc-like orientation, $\phi^{(\alpha)} = (+30°, 90°, -30°)$, the situation is opposite: the A–B and C–D sector boundaries are normal to the inclined slip planes, while the B–C boundary is parallel to the $\phi^{(2)} = 90°$ planes. Hence, this solution implies a shear band along the B–C sector boundary and kink bands along the A–B and C–D boundaries.

Although the discrete dislocation simulations to be discussed subsequently involve some strain hardening, we will make reference to the non-hardening crystal plasticity solutions for simplicity. Saeedvafa and Rice (1989) have shown that the simple picture changes when hardening is accounted for. The solution then leads to seven sectors. The stress states in three of these are on the vertices of the yield surface, corresponding to double slip, and on flat segments in the remaining sectors, thus involving only a single slip. Also, the displacement field becomes continuous rather than discontinuous across sector boundaries, but these still correspond to regions of localized strain.

3.2. Discrete dislocation results

In this section, we discuss the discrete dislocation simulation results for the fcc- and bcc-like crystal orientations. Unless otherwise specified, the results correspond to a dislocation source density of 78 μm^{-2}. Fig. 3 shows the dislocation distributions for the two crystal orientations at levels of the applied stress intensity factors such that the plastic zone spans a large part of the process window. The crack-opening profiles show that substantial blunting has taken place. Careful examination of these distributions reveals many dislocations on the $\phi^{(3)} = 60°$ slip plane for the fcc-like orientation, in Fig. 3a, and on the $\phi^{(2)} = 90°$ planes for the bcc-like orientation in Fig. 3b. Both suggest strong shearing along these planes, which is consistent with Rice's (1987) continuum plasticity result discussed above. In addition, many dislocations are present on the $\phi^{(2)} = 0°$ planes in the region $60° < \theta < 120°$ for the fcc-like orientation. While this is reminiscent of the kinking mechanism that follows from the continuum analysis, it differs because it involves dislocations gliding over relatively large distances which does not lead to strain localization in a kink band. However, in the bcc-like orientation there is some evidence of dislocation concentrations on the $\phi^{(3)} = -30°$ planes in the $55° < \theta < 75°$ region which is suggestive of a kink band as in the continuum solution of Rice (1987).

Further insight into the deformation mechanisms is provided by the stress distributions, shown in Figs. 4 and 5 for the two orientations at $K_I = 0.6\ \mathrm{MPa}\sqrt{\mathrm{m}}$. They exhibit turbulent stress fluctuations, which are due to the singularities of the individual dislocations. In fact, the fluctuations are actually damped in the figure because of

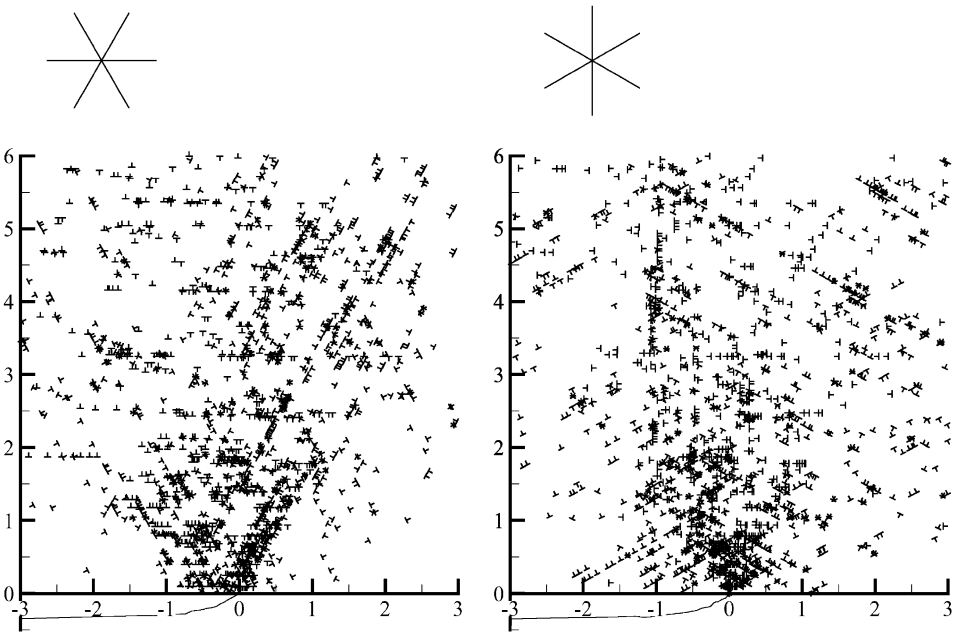

Fig. 3. Distributions of dislocations around the crack tip in a crystal with slip systems at (a) $\phi^{(\alpha)} = (-60°, 0, +60°)$ and (b) $\phi^{(\alpha)} = (+30°, 90°, -30°)$ for $K_I = 0.6\,\mathrm{MPa}\sqrt{\mathrm{m}}$. The corresponding crack-opening profiles (displacements magnified by a factor of 10) are plotted below the x_1-axis.

the way the contours are plotted on the finite element mesh that was used for the computation (80×80 elements in the process window). The figure reiterates the key finding by Cleveringa et al. (2000) that the stresses in the immediate vicinity of the crack tip grow very large with increasing K_I over distances that are much larger than the average dislocation spacings. Further away from the immediate crack tip region, the stresses are significantly lower on average.

For the fcc-like orientation, the stress distributions in Fig. 4 optically suggest three sectors inside which the stresses are, on average, rather constant. The boundaries are roughly oriented at $+60°$ and $120°$ from the crack plane, which is consistent with the A–B and C–D sector boundaries of Rice's (1987) solution in Fig. 2b. A third sector boundary at 90°, corresponding to the kink band, is not immediately obvious from Fig. 4. On the other hand, for the bcc-like orientation we see boundaries oriented at roughly $+60°$ and 90° from the σ_{11} and σ_{22} stress distributions. Further, a boundary at about $120°$ is observed from the σ_{12} contour plot.

3.2.1. Comparison with Rice's (1987) *continuum solutions*

Having found that, at least visually, three of the four sectors in the continuum slip solution of Rice (1987) can be observed in the discrete dislocation results for the fcc-like orientation, we now carry out a quantitative comparison. For this purpose, the

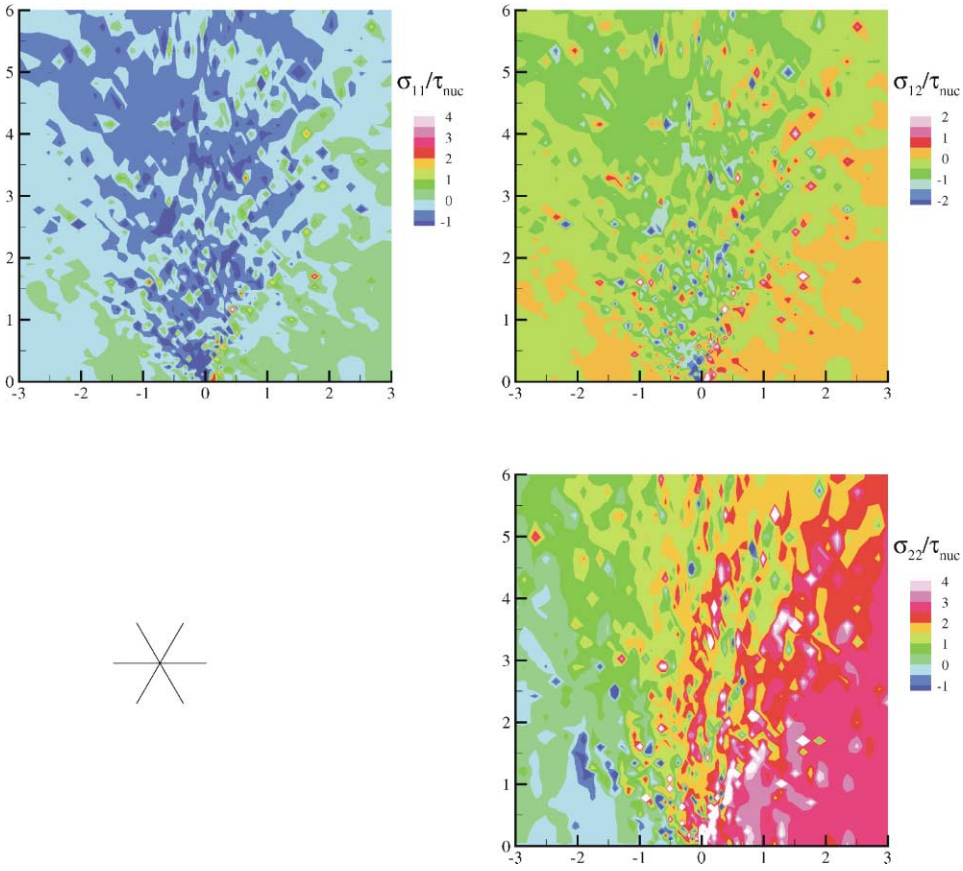

Fig. 4. Stress distributions, normalized by the nucleation strength τ_{nuc}, for the fcc-like orientation $\phi^{(\alpha)} = (-60°, 0°, +60°)$ as in Fig. 3a at $K_I = 0.6\ \mathrm{MPa}\sqrt{\mathrm{m}}$.

stress fields are averaged inside the four sectors, in an annular region with an inner radius of 0.5 μm and an outer radius of 1.5 μm. This is a compromise choice which ensures that averaging is performed inside the plastic zone for the higher load levels, as shown in Fig. 4, but excludes the highly stressed near-tip region. Fig. 6 shows the sector-averaged stresses with the increasing applied K_I, in order to illustrate the development of plasticity. To give some idea about statistical effects, stresses corresponding to a second source and obstacle realization are shown along with the distribution shown in Fig. 4. The differences between the stresses for the two realizations are small and roughly equal to the fluctuations with the increasing K_I in all cases. The evolution of the sector-averaged opening stress suggests that plasticity in this ring-shaped region around the crack tip initiates around $K_I = 0.2\ \mathrm{MPa}\sqrt{\mathrm{m}}$. For values of K_I that exceed about two times this value, the stresses more or less level out, consistent with the non-hardening continuum slip solution.

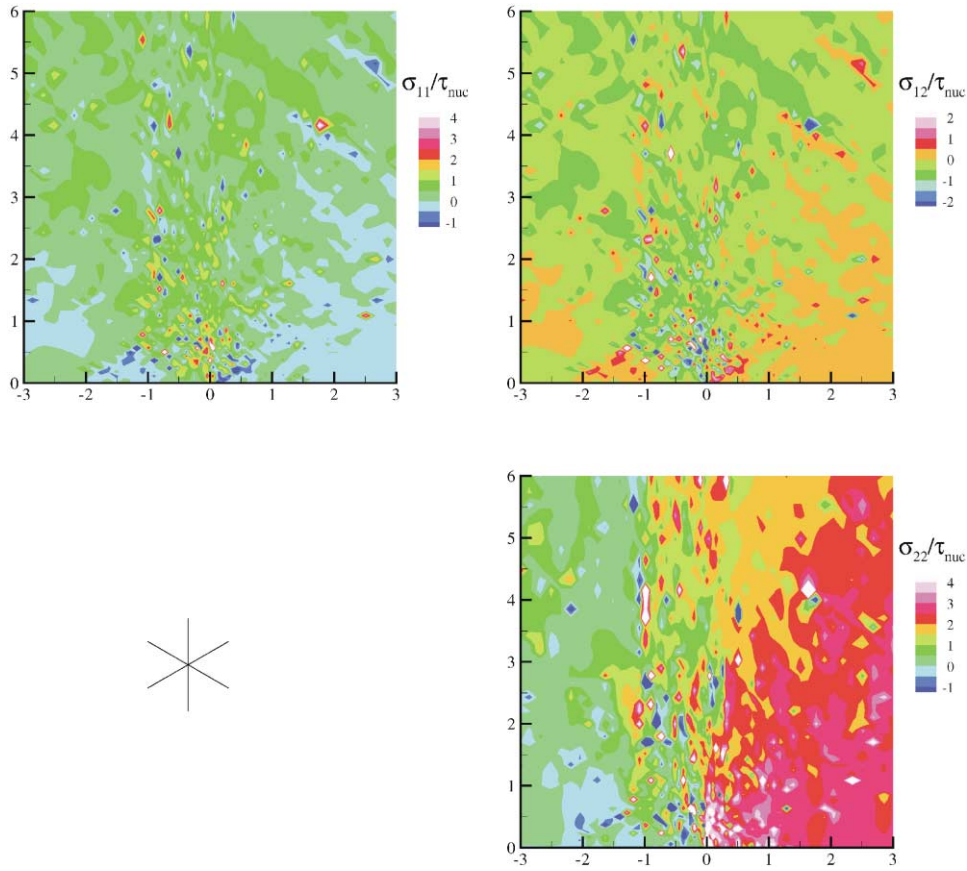

Fig. 5. Stress distributions, normalized by the nucleation strength τ_{nuc}, for the bcc-like orientation $\phi^{(\alpha)} = (+30^\circ, 90^\circ, -30^\circ)$ as in Fig. 3b at $K_{\text{I}} = 0.6\,\text{MPa}\sqrt{\text{m}}$.

We compare these sector-averaged stresses with the non-hardening continuum slip solution by fitting the value of the yield stress τ_0 so that the opening stress in sector A at the largest $K_{\text{I}} = 0.6\,\text{MPa}\sqrt{\text{m}}$ agrees with the value from Table 1; this gives $\tau_0 = 0.49\tau_{\text{nuc}}$. Comparing then the continuum stress levels with the dislocation results at $K_{\text{I}} = 0.6\,\text{MPa}\sqrt{\text{m}}$, we see from Fig. 6 that the stresses σ_{22} and σ_{12} agree rather well except in sector C where the absolute values of the dislocation stresses are almost a factor two higher. The continuum and discrete dislocation predictions of σ_{11} are in good agreement in all sectors.

The average stresses over the sectors in Rice's (1987) solution as obtained from our discrete dislocation simulations for the bcc-like orientation are shown in Fig. 7. Again we see that the stresses level out at about $K_{\text{I}} = 0.4\,\text{MPa}\sqrt{\text{m}}$. We compare these stresses with Rice's (1987) solution taking $\tau_0 = 0.45\tau_{\text{nuc}}$. From Fig. 7, we see that the discrete dislocation simulations agree with this continuum solution except that σ_{22}

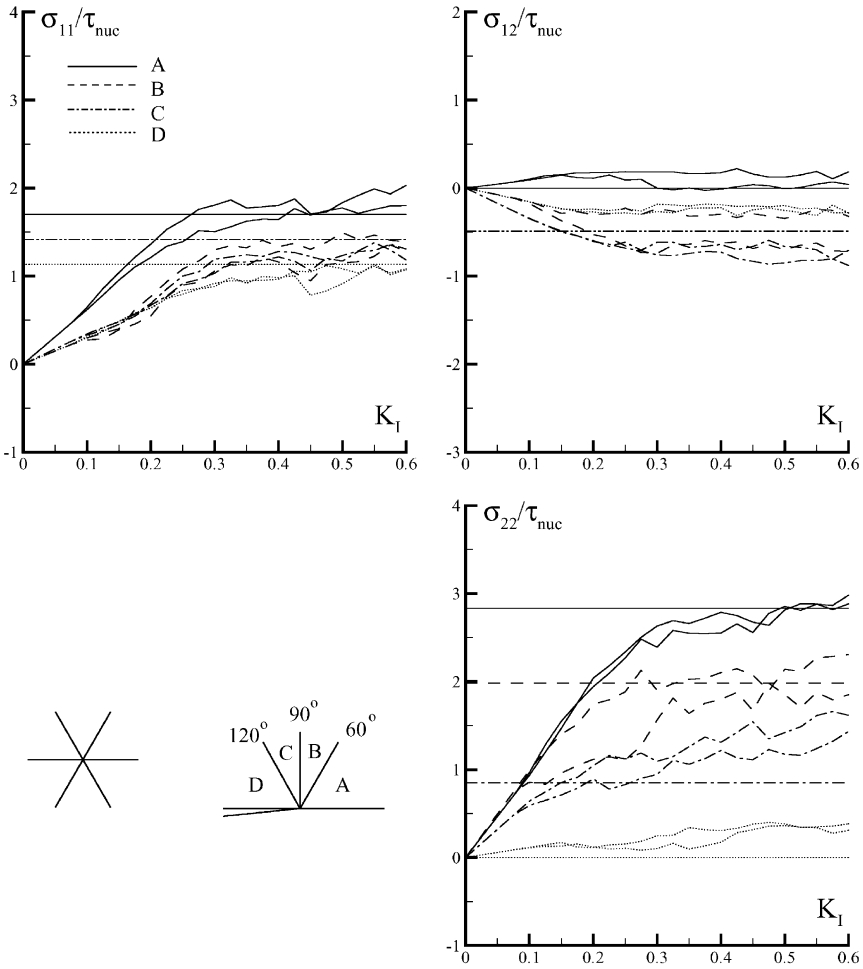

Fig. 6. Sector-averaged stresses as a function of the applied K_I (in MPa$\sqrt{m}$) for the fcc-like orientation. The sectors are shown in the inset. The results of two realizations of sources and obstacles are shown. The straight horizontal lines correspond to Rice's (1987) continuum solution in Table 1 taking $\tau_0 = 0.49\tau_{nuc}$. Note that some stress components in the continuum plasticity solution have the same value in more than one sector.

in sector B is underpredicted by the continuum solution. To explore statistical effects, a calculation was carried out using a second source and obstacle realization for the bcc-like geometry. The results did not differ substantially from those shown here and are omitted for the sake of brevity.

Average stress comparisons provide coarse measures for ascertaining the agreement between the continuum and the discrete dislocation simulation results. It is also necessary for the discrete dislocation results to show kink and slip bands at the appropriate angles. Thus, we proceed to analyze the strain distributions obtained from

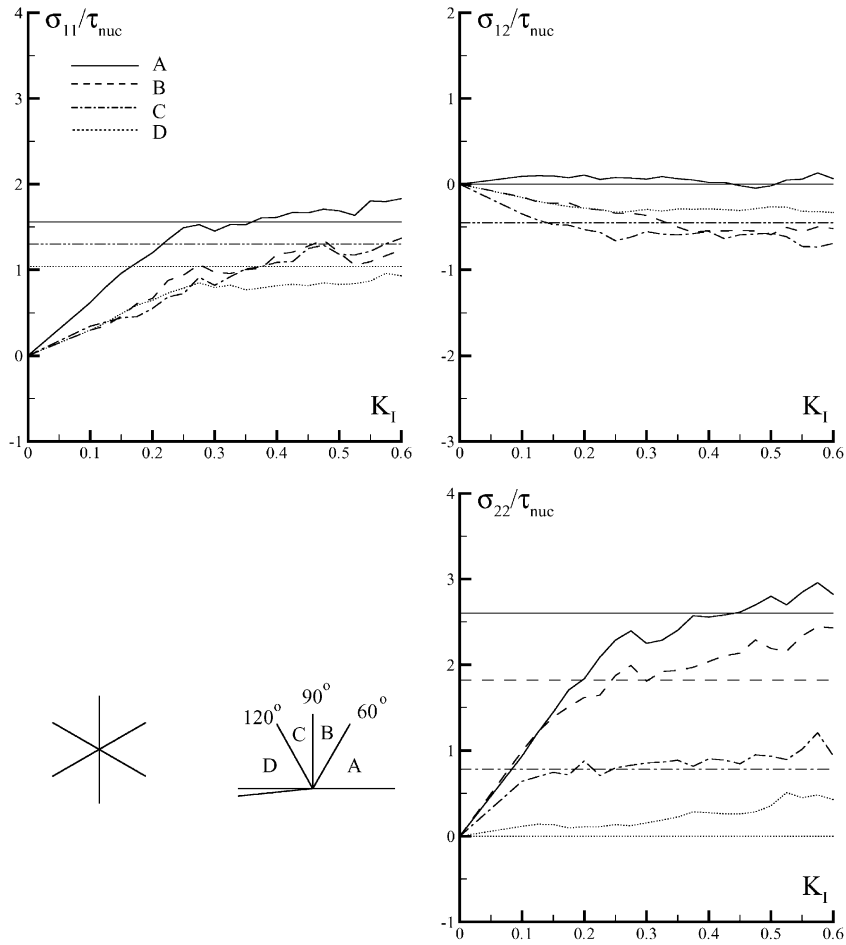

Fig. 7. Sector-average stresses as a function of the applied K_I (in MPa$\sqrt{\text{m}}$) for the bcc-like orientation. The sectors are shown in the inset. The straight horizontal lines correspond to Rice's (1987) continuum solution in Table 1 taking $\tau_0 = 0.45\tau_{nuc}$. Note that some stress components in the continuum plasticity solution have the same value in more than one sector.

the discrete dislocation simulations, as shown in Figs. 8 and 9. These strains ε_{ij} are obtained by numerical differentiation of the total displacement field $u_i = \tilde{u}_i + \hat{u}_i$ using nodal values of the displacements on the finite element mesh. This results in the localized strains associated with the slips being smeared out to some extent. Nevertheless, the fcc-like results in Fig. 8 clearly reveal that plastic deformation occurs by several slip bands parallel to the 60° slip planes, clustered in a band of about 1 μm thickness. The distribution of ε_{12} shows the evidence of slip on planes parallel to the crack plane up to about 3 μm away from the crack face in the region $60° < \theta < 120°$. However, no evidence of concentrated shear reminiscent of a kink band is seen. The strain dis-

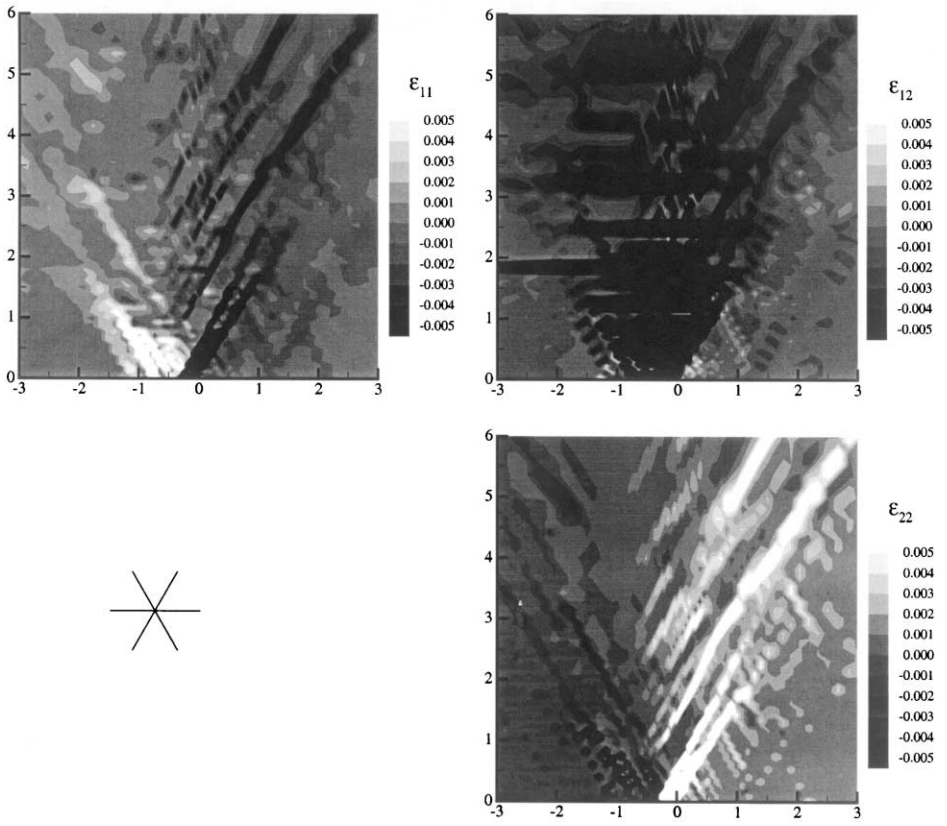

Fig. 8. Strain distributions for the fcc-like orientation corresponding to the case shown in Fig. 3a.

tributions for the bcc-like orientation, Fig. 9, clearly show strong slip activity on the 90° slip planes above the crack, and some evidence of kink bands at 60° and 120°.

Fig. 10 shows the trajectory in strain space of the average total strains in the annular region between $r = 0.5$ and 1.5 μm from $\theta = 0°$, in front of the crack, to $\theta = 180°$. Fig. 10a, for the fcc-like orientation, shows a distinct peak around $\theta = 60°$, which is consistent with the localized deformation along the A–B sector boundary in the continuum solution of Rice (1987). However, unlike Rice's (1987) solution, there is no evidence of localized deformation in a kink band at $\theta = 90°$ or in a slip band at $\theta = 120°$. For the bcc-like orientation (Fig. 10b), we see strong evidence of localized deformation at $\theta \approx 80°$ and 100° and a smaller band at $\theta \approx 130°$. The strong localized deformation seen between 90° and 100° corresponds to the slip band in Rice's (1987) solution. The 80° and 130° localized bands correspond to emerging kink bands, but are not seen exactly at the expected angles of 60° and 120° as the kink bands formed in the discrete dislocation simulations are diffused. Thus, the results for the fcc-like orientation differ from Rice's (1987) continuum plasticity solu-

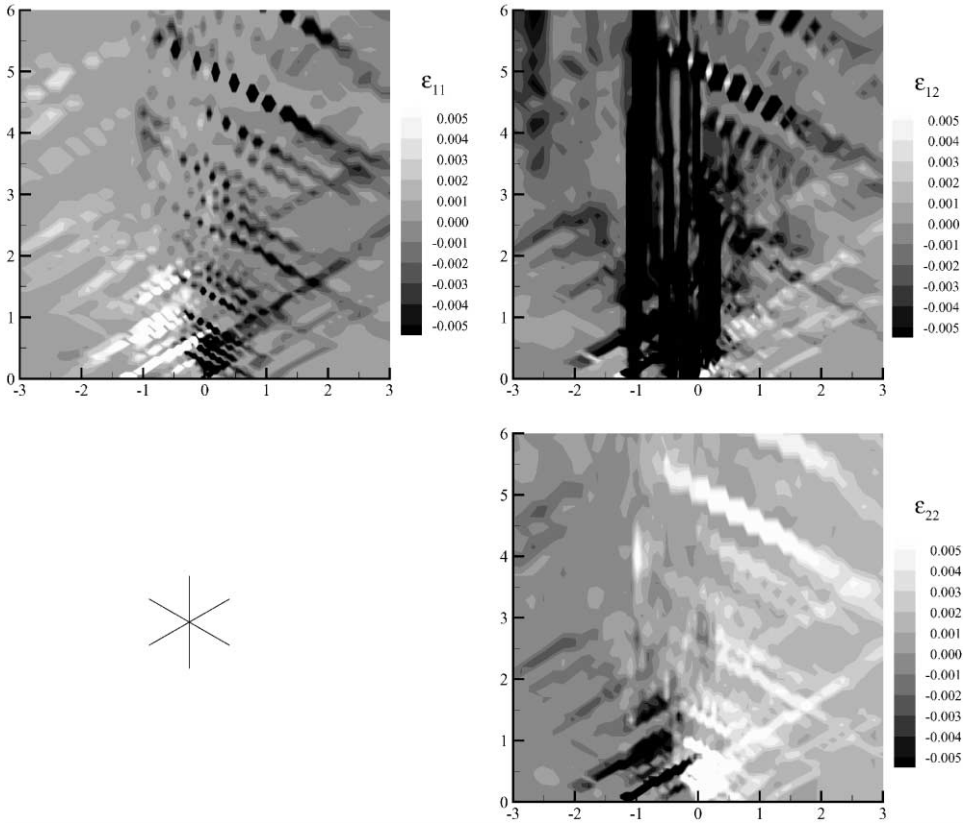

Fig. 9. Strain distributions for the bcc-like orientation corresponding to the case shown in Fig. 3b.

tion while the results for the bcc-like orientation are in reasonable agreement with his predictions.

With a lower density of dislocation sources, fewer dislocations can be generated to accommodate the deformations by kink bands and it is expected, Rice (1987), that for a sufficiently low source density, kink bands will be suppressed. To explore this, we have repeated the bcc-like calculation with a source density of 46 μm^{-2} instead of 78 μm^{-2}. The resulting strain space plot in Fig. 10c shows that with the lower source density there is no evidence of strain peaks at the kink band angles of approximately 60° and 120°.

3.2.2. Comparison with Drugan's (2001) continuum slip analysis

Discrete dislocation solutions have been obtained for both the fcc- and bcc-like orientations that show no evidence of kink bands. The non-hardening continuum slip solutions are not unique and Drugan (2001) has constructed alternative elastic-ideally plastic solutions in which kink bands do not form. His analyses are carried out for true fcc and bcc orientations, but can be re-analyzed for the orientations used in the

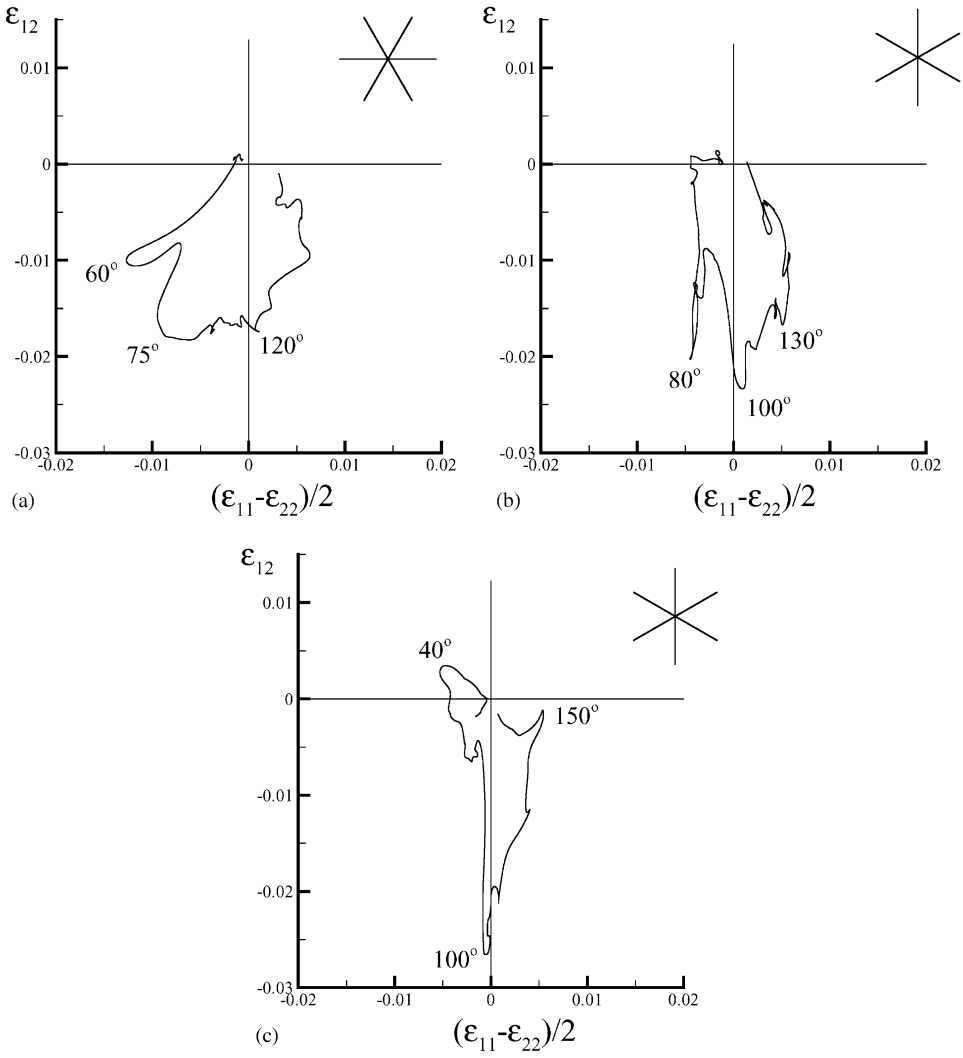

Fig. 10. Strain space plots at $K_I = 0.6\ \mathrm{MPa}\sqrt{\mathrm{m}}$ averaged in the radial direction between 0.5 and 1.5 μm from the crack tip: (a) fcc-like orientation with a source density 78 μm^{-2}, (b) bcc-like orientation with a source density 78 μm^{-2} and (c) bcc-like orientation with a source density 46 μm^{-2}. A few typical values of θ are given to help interpret the circumferential variation of the strains.

discrete dislocation calculations (Fig. 1b); it is these re-analyzed solutions that we describe below.

For the fcc-like orientation, Drugan (2001) found several solution families without kink bands. We consider a family of solutions which involve only a slip band at θ=60°; consistent with our discrete dislocation simulations. Drugan (2001) showed that such a family of solutions has a sector configuration similar to that in the solution of Rice

Table 2
Stress states in the three sectors of Drugan's (2001) solution (see Fig. 11) for the fcc-like orientation with an elastic discontinuity at $\theta = 105°$

Sector	σ_{22}/τ_0	σ_{11}/τ_0	σ_{12}/τ_0
A	$2\sqrt{3}+2$	$2/\sqrt{3}+2$	0
B	$\sqrt{3}+2$	$1/\sqrt{3}+2$	-1
D	0	$4/\sqrt{3}$	0

(1987) (Fig. 2b) but with sector C being an elastic sector rather than plastic. The two limiting cases in his family of solutions are:

(i) An elastic sector C for $90° \leqslant \theta \leqslant 120°$. The stress levels according to this solution differ only very slightly from Rice's (1987) solution in Table 1.
(ii) The elastic sector C collapsing to a line elastic discontinuity at $\theta = 105°$. The stress levels according to this solution are given in Table 2.

The absence of a dislocation-free sector in the discrete dislocation results, Fig. 3a, seems to exclude the solution with a finite elastic sector C. It is thus instructive to compare the stress levels from our computations with Drugan's (2001) solution in the limiting case of the line elastic discontinuity. Fig. 11 shows this comparison for the choice $\tau_0 = 0.51\tau_{\text{nuc}}$. The two solutions agree very well in all sectors.

Drugan (2001) has proposed a number of families of kink band free solutions for the bcc orientation. Since our bcc-like orientation results for a source density of 46 μm^{-2} do not exhibit kink bands, we examined these in light of several of Drugan's (2001) solutions; none agreed particularly well with our discrete dislocation simulation results. Here, we present a comparison with the solution that produced the best match. This solution involves five sectors, which are shown in the inset of Fig. 12, with uniform stress states indicated by letters corresponding to Fig. 2a. The stress levels are given in Table 3. The solution proposed by Drugan (2001) has the sector behind the crack tip for $180° > \theta > 150°$ below yield, with all stress components being identically equal to zero. Probably the most fascinating element of this solution is the sector in between sectors A and B, where the stress state is located infinitesimally above A on the yield surface (Fig. 2a). This is in fact a limiting case of a family of solutions where this sector is on the yield surface somewhere between A and F. It implies that the plastic strain rate $\dot{\varepsilon}^{\text{p}}_{12}$ is positive in this sector, which is consistent with the strain map for the discrete dislocation results in Fig. 10c. Fig. 12 shows the comparison with the sector-averaged stresses found in the discrete dislocation analysis. There are several possibilities for the lack of agreement:

(i) There may be another member of the family of possible non-hardening solutions which gives a better match and which we have missed (however, we think this is unlikely).
(ii) With the low source density, a higher value of K_{I} may be needed before the fully plastic state is reached. To check this we ran a calculation to $K_{\text{I}} = 1.0\ \text{MPa}\sqrt{\text{m}}$.

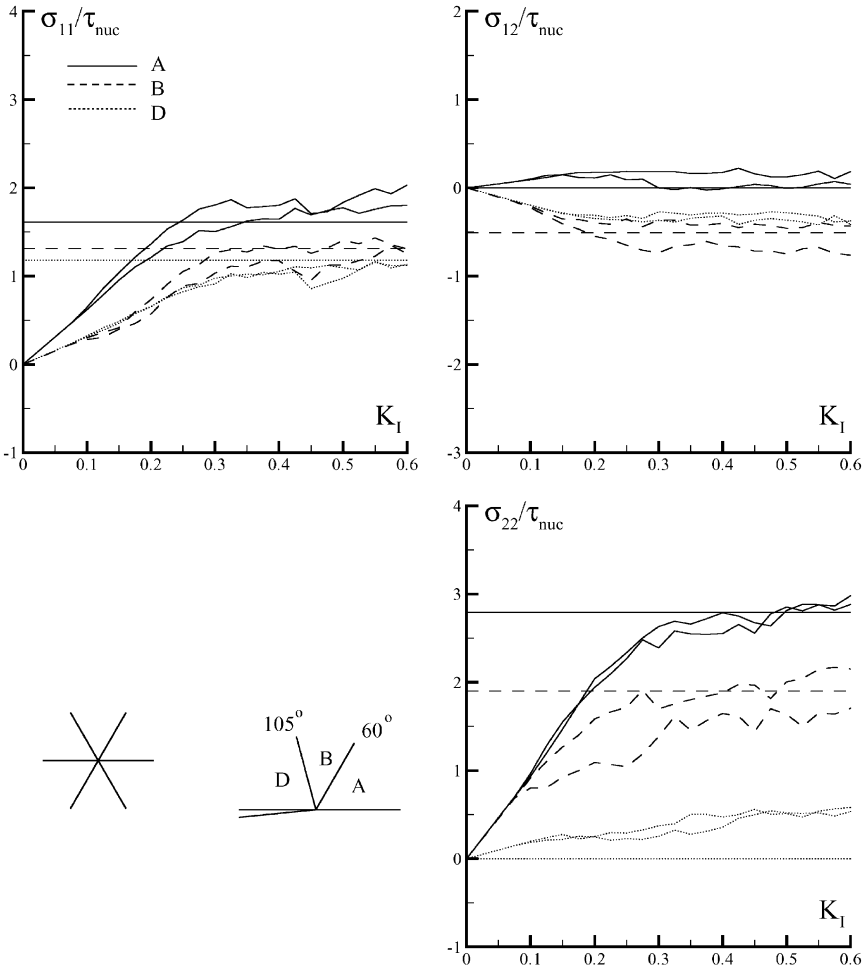

Fig. 11. Sector-averaged stresses as a function of the applied K_I (in MPa$\sqrt{m}$) for the fcc-like orientation. The sectors are shown in the inset. The results of two realizations of sources and obstacles are shown. The straight horizontal lines correspond to Drugan's (2001) continuum solution with the line elastic discontinuity at 105° (Table 2) and with $\tau_0 = 0.51\tau_{nuc}$.

However, no improvement in the agreement with the non-hardening continuum predictions was found.

(iii) Strain hardening effects may be more prominent with a lower dislocation source density. The calculation carried out to $K_I = 1.0$ MPa$\sqrt{m}$ showed that some of the sector average stresses did not level out and continued to increase with increasing K_I. This suggests that this discrete dislocation simulation should be compared with a strain-hardening continuum solution.

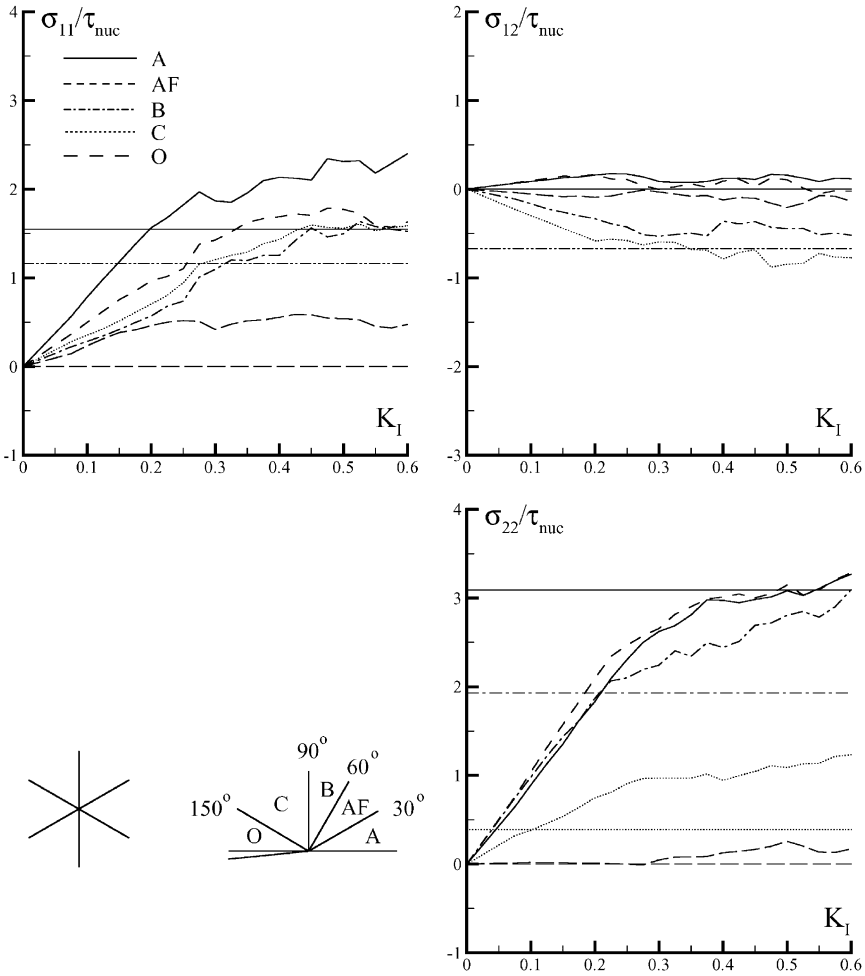

Fig. 12. Sector-averaged stresses as a function of the applied K_I (in MPa$\sqrt{\text{m}}$) for the bcc-like orientation with a source density of 46 μm^{-2}. The sectors are shown in the inset. The straight horizontal lines correspond to Drugan's (2001) continuum solution in Table 3 taking $\tau_0 = 0.67\tau_{nuc}$. Note that some stress components in the continuum plasticity solution have the same value in more than one sector.

4. Concluding remarks

Discrete dislocation solutions have been obtained for crack tip fields in planar model crystals. Two orientations were considered; one fcc-like and the other bcc-like. Sources for dislocation nucleation were distributed throughout the process region with no special nucleation from the crack tip. For a high dislocation source density, the stress fields in the plastic zone, away from the immediate crack tip region, are reasonably well described by non-hardening continuum slip solutions; for the fcc-like orienta-

Table 3
Stress states in the five sectors of Drugan's (2001) solution (see Fig. 12) for the bcc-like orientation

Sector	σ_{22}/τ_0	σ_{11}/τ_0	σ_{12}/τ_0
A	$8/\sqrt{3}$	$4/\sqrt{3}$	0
AF	$8/\sqrt{3}$	$4/\sqrt{3}$	0
B	$5/\sqrt{3}$	$\sqrt{3}$	-1
C	$1/\sqrt{3}$	$\sqrt{3}$	-1
O	0	0	0

tion, the agreement is closer with Drugan's (2001) kink band free solution, while for the bcc-like orientation the dislocation predictions give evidence for the emergence of kink bands and are in closer agreement with the solution of Rice (1987). Note that the stress states corresponding to the solutions of Rice (1987) and Drugan (2001) for the fcc-like geometry are not that different. The main difference is in the predicted deformation state: with or without kink bands. By contrast, for the low source density bcc-like orientation we found no non-hardening continuum solution to be in good agreement with our discrete dislocation simulation. We attribute this mainly to hardening effects that play a significant role in the low source density case.

The development of a kink band deformation mode was found to depend on the crystal geometry and on the dislocation source density. More generally, the emergence or not of kink bands may also depend on other parameters of the dislocation description such as the active slip plane spacing, the distribution and strength of dislocation sources, etc. Indeed, as noted by Rice (1987), kink bands require an abundant number of dislocation sources to be activated. It is worth noting that while experiments on Cu fcc single crystals (Crone and Shield, 2001) show slip bands but not kink bands in the crack tip fields, experiments on dislocation source rich Fe–Si bcc single crystals (Shield and Kim, 1994) show some evidence of the possible emergence of kink bands in the crack-tip fields. Calculations analogous to those carried out here, but for actual fcc and bcc crystal geometries, would be useful in exploring circumstances that permit kink band formation.

The very high local stresses that develop in the immediate vicinity of the crack tip are not reproduced by any solution based on conventional continuum plasticity. These high stresses eventually lead to crack propagation at cohesive strengths that are approaching the atomic bond strength (Cleveringa et al., 2000). Various non-local theories of plasticity have been proposed to account for the increased strength associated with plastic flow in small volumes, e.g. Aifantis (1984), Fleck et al. (1994), Fleck and Hutchinson (1997), Gao et al. (1999), Acharya and Bassani (2000), Gurtin (2000). An isotropic non-local plasticity theory that associates this strength increase with geometrically necessary dislocations does raise stress levels in the vicinity of a crack tip (Wei and Hutchinson, 1997). A similar analysis for crack tip fields in a crystalline solid permits a direct comparison with the discrete dislocation predictions for the stress elevation and allows non-local effects on the emergence of kink bands

to be explored. Indeed, the Cosserat continuum calculations by Forest et al. (2001) indicate that including hardening due to lattice curvature favors slip bands over kink bands.

Acknowledgements

We are grateful for support from the Materials Research Science and Engineering Center on *On Micro-and-Nano-Mechanics of Electronic and Structural Materials* at Brown University (NSF Grant DMR-0079964). The work of H.H.M. Cleveringa was further supported by the "Stichting voor Fundamenteel Onderzoek der Materie (FOM)" which is part of the "Nederlandse Organisatie voor Wetenschappelijk Onderzoek (NWO)". It is a pleasure to acknowledge enlightening discussions with Prof. W.J. Drugan.

References

Acharya, A., Bassani, J.L., 2000. Incompatibility and crystal plasticity. J. Mech. Phys. Solids 48, 1565–1595.

Aifantis, E.C., 1984. On the microstructural origin of certain inelastic models. J. Eng. Mater. Technol. 106, 326–330.

Cleveringa, H.H.M., Van der Giessen, E., Needleman, A., 2000. A discrete dislocation analysis of mode I crack growth. J. Mech. Phys. Solids 48, 1133–1157.

Cuitiño, A.M., Ortiz, M., 1992. Computational modelling of single crystals. Modelling Simulation Mater. Sci. Eng. 1, 225–263.

Crone, W.C., Shield, T.W., 2001. Experimental study of the deformation near a notch tip in copper and copper–beryllium single crystals. J. Mech. Phys. Solids, in press.

Drugan, W.J., 2001. Asymptotic solutions for tensile crack tip fields without kink-type shear bands in elastic-ideally plastic single crystals. J. Mech. Phys. Solids 49, 2155–2176.

Fleck, N.A., Hutchinson, J.W., 1997. Strain gradient plasticity. Adv. Appl. Mech. 33, 295–361.

Fleck, N.A., Muller, G.M., Ashby, M.F., Hutchinson, J.W., 1994. Strain gradient plasticity: theory and experiment. Acta Metall. Mater. 42, 475–487.

Forest, S., Boubidi, P., Sievert, R., 2001. Strain localization patterns at a crack tip in generalized single crystal plasticity. Scripta Mater. 44, 953–958.

Freund, L.B., 1994. The mechanics of dislocations in strained-layer semiconductor-materials. Adv. Appl. Mech. 30, 1–66.

Gao, H., Huang, Y., Nix, W.D., Hutchinson, J.W., 1999. Mechanism-based strain gradient plasticity—I. Theory. J. Mech. Phys. Solids 47, 1239–1263.

Gurtin, M., 2000. On plasticity of crystals: free energy, microforces, plastic strain gradients. J. Mech. Phys. Solids 48, 989–1036.

Hutchinson, J.W., 1968. Singular behaviour at the end of a tensile crack in a hardening material. J. Mech. Phys. Solids 16, 13–31.

Needleman, A., 1990. An analysis of tensile decohesion along an interface. J. Mech. Phys. Solids 38, 289–324.

Rice, J.R., 1987. Tensile crack tip fields in elastic-ideally plastic crystals. Mech. Mater. 6, 317–335.

Rice, J.R., Rosengren, G., 1968. Plane strain deformation near a crack tip in a power-law hardening material. J. Mech. Phys. Solids 16, 1–12.

Rose, J.H., Ferrante, J., Smith, J., 1981. Universal binding energy curves for metals and bimetallic interfaces. Phys. Rev. Lett. 47, 675–678.

Saeedvafa, M., Rice, J.R., 1989. Crack tip singular fields in ductile crystals with Taylor power-law hardening. II: plane strain. J. Mech. Phys. Solids 37, 673–691.

Shield, T.W., Kim, K.-S., 1994. Experimental measurement of the near tip strain field in an iron–silicon single crystal. J. Mech. Phys. Solids 42, 845–873.

Van der Giessen, E., Needleman, A., 1995. Discrete dislocation plasticity: a simple planar model. Modelling Simulation Mater. Sci. Eng. 3, 689–735.

Wei, Y., Hutchinson, J.W., 1997. Steady-state crack growth and the work of fracture for solids characterized by strain gradient plasticity. J. Mech. Phys. Solids 45, 1253–1273.